IEEE Robotics and Automation Letters (RA-L) paper, presented at ICRA 2026, Vienna, Austria. Cite as RA-L paper.

Motion Control and Power Distribution of H-shaped Multi-modal Transformable Rotorcraft

Wang Xuqiao[1,*], Guo Da[1,2], Zhao Changli[3], Duan Menghao[1], Luo Qijun[1]

Abstract— Multilink transformable rotorcraft demonstrate exceptional flexibility when navigating confined spaces, yet face critical challenges including time-varying center of gravity, body misalignment, and the absence of a unified control strategy during dynamic reconfiguration, which severely restrict motion continuity and operational capability. To address these limitations, we propose an H-shaped multi-modal transformable rotorcraft. Its novelty lies in utilizing a designed H-shaped variable structure with 6 controllable degrees of freedom (CDOF), achieving a balance between structural flexibility and the resolution of time-varying center-of-gravity limitations. It proposes a control parameter tuning method based on motion characteristic values and a power distribution route based on the principle of competence. Under limited computational overhead, it realizes narrow-gap flight and single-propeller power failure response through dynamic configuration reconstruction. Experimental results demonstrate that our platform successfully overcomes stability challenges, achieving a position deviation of less than 4 cm when traversing constrained spaces, it can reduce its lateral width by more than 50% , and can switch to a fault-tolerant configuration within 1.2 s to respond to sudden single-propeller power failures while maintaining stable flight. Additionally, it possesses torque output capability for twist operations during manipulation tasks. The H-shaped transformable rotorcraft enables multi-modal morphing control and smooth power transitions, providing a versatile platform for multi-scenario flight operations.

I. Introduction

Traditional rotorcraft are widely adopted for their simplicity and mature control [1]. Research on scenario-specific operations typically follows two approaches [2]: adding extension mechanisms (e.g., protective shells [3], robotic arms [4], or wheels [5]), adding pole frames to enhance attachment and habitat capabilities [6], [7], or implementing variable structure designs (e.g., folding airframes [8] or tilt-rotors [9]).

Morphing technology has gained sustained attention as an effective means to enhance adaptability in complex environments [10]–[12]. As summarized in Table I, existing transformable rotorcraft offer varying capabilities: some provide precise control with significant size reduction (e.g., 48.1% in [13]), while others enable sustained throughput and object transport [14]–[20].

Multi-link structures offer excellent flexibility; however, during dynamic reconfiguration, their center of gravity does not remain coincident with the geometric center of the airframe. This time-varying center of gravity makes it challenging to ensure flight stability, thereby limiting motion continuity and overall performance. To address these limitations, this work proposes an H-shaped multi-modal transformable rotorcraft. The main contributions of this work include the following three aspects:

TABLE I
Comparison of Related Works on Transformable Rotorcraft

Feature	[13]	[14]-[15]	[16]–[19]	[20]	This work
CDOF	4	2	7	8	6
Passability	✓	✓	✓	✓	✓
Transport	×	✓	✓	✓	✓
Full-actuated	×	×	×	✓	✓
Torque-output	×	×	×	✓	✓
Fault-tolerant	×	×	×	×	✓

- A deformable structure with an H-shaped baseline configuration was designed, achieving a balance between structural flexibility and the resolution of time-varying center-of-gravity [21] limitations.
- A control parameter tuning method based on motion characteristic values and a power distribution strategy based on competency principles were proposed. With limited computational overhead, the feasibility of constrained-space motion and single-rotor power failure response was validated through dynamic reconfiguration of the configuration.

This article is organized as follows: Section II details the structural design and deformation mechanism; Section III presents the motion modeling, control, and power distribution methods; Section IV experimentally validates the multi-modal motion capabilities; and Section V concludes the paper.

II. Structural Design and Deformation Mechanism

A. Design Principles

1) During the process of rotorcraft configuration reconstruction, the center of gravity should be kept close to the body and avoid time-varying.
2) Minimize the number of movable joints to avoid excessive flexibility in system movement.
3) Consider control redundancy and provide fault-tolerant flight conditions.
4) Achieve structural support for system capability acquisition or performance improvement with as few structural components as possible.

B. Structural Design and Specifications

As shown in Fig. 1, the rotorcraft features a fuselage with two arms connected at its endpoints, enabling horizontal rotation for reconfiguration. Each arm carries

two brushless motors at its ends, arranged in diagonally paired groups with opposing rotation directions. Four tilting servos allow motor rotation perpendicular to the arms, generating horizontal forces to compensate for torque deficiencies during structural changes. All flight control components are centralized at the fuselage midpoint, coinciding with the center of gravity.

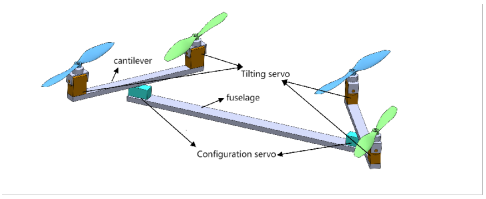

Fig. 1. Structure diagram of the rotorcraft.

C. Deformation Mechanism

1) Configuration Characteristics: The rotorcraft achieves multi-modal flight by rotating its arms around the fuselage endpoints, primarily operating in three typical configurations: H, T, and I. Crucially, each of these configurations is designed to satisfy static stability conditions, ensuring sufficient control torque and attitude stability for autonomous flight.

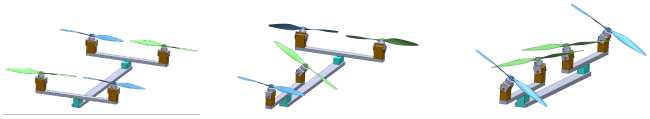

(a) H-shape (b) T-shape (c) I-shape

Fig. 2. Three operating modes of the transformable rotorcraft.

- H-configuration (General Flight): The symmetric H-shape provides balanced and maximum lever arms for pitch, roll, and yaw control, offering stable flight performance akin to a conventional quadrotor.
- T-configuration (Fault-tolerant Flight): In this configuration, the three active motors form a triangular layout. This arrangement ensures that the center of gravity (CoG) lies within the triangle formed by the effective thrust vectors, which is a fundamental prerequisite for stable flight under single-propeller failure.
- I-configuration (Crossing Flight): The linear arrangement minimizes the lateral footprint for crossing narrow gaps. Static stability is maintained by actively tilting the rotors to generate the necessary control moments, compensating for the reduced roll arm.

2) Safe Reconfiguration Channel: A critical guarantee for stable dynamic reconfiguration is that the CoG must remain within the effective area enclosed by the thrust vectors of all active motors throughout the transformation process. Our structural design and deformation rules are inherently guided by this principle. As illustrated in Fig. 3 and the subsequent transformation diagrams, the predefined transformation sequences (e.g., H-I parallelogram/trapezoid transition, H-T/I-T failure response) are designed to strictly constrain the CoG within this safe region. From an engineering practicality standpoint, adhering to these predefined morphing sequences establishes a safe reconfiguration channel, thereby ensuring continuous flight stability and controllability during transitions.

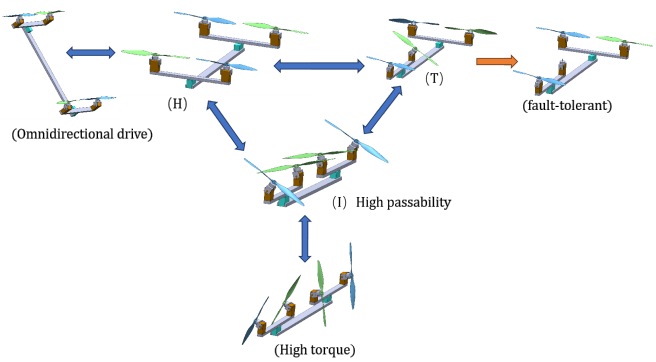

Fig. 3. Rotorcraft deform mode.

a) Continuous Motion in Confined Space (H-I): Rotorcraft typically fly in the H-configuration as their general configuration. When encountering a narrow gap and needing to fly through continuously, the rotorcraft deforms into the I configuration. According to the motor thrust calculation, when the absolute value of the angle between the arm and the fuselage is 30°, the roll moment arm is reduced to 1/2, and the tilt servo needs to start rotating to compensate for the lost roll moment.

The transition of the rotorcraft configuration from H to I can be achieved in two ways. As shown in Fig. 4a, during the transition in a parallelogram configuration, the tilt servo angles should be adjusted in two ways. The servo away from the center of gravity should have a smaller tilt angle, while the servo closer to the center of gravity should have a larger tilt angle, thus ensuring that the absolute values of the yaw moment arms are equal. As shown in Fig. 4b, during the transition in an isosceles trapezoid configuration, the tilt servo angles can remain at a constant value to balance the yaw moment arms.

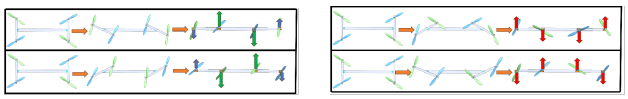

(a) H-configuration (b) T-configuration

Fig. 4. Diagram of H-I transformation in configuration.

Yaw torque arises from two sources: the fixed-direction reverse torque from motor rotation, and the bidirectional yaw torque from motor tilting. In order to avoid the phenomenon of mutual cancellation between the two, the yaw torque generated by the tilting of the motor needs to be consistent with the direction of the reverse torque.

During the aforementioned configuration transformation process, the reduction in the coupling parameter does not exceed the original 1/2 and does not change its sign, resulting in a feasible solution. It is worth noting that the transition transformation rules are not unique, and the above two transformation rules are primarily based on design adherence.

b) Response to Single-Propeller Power Failure (H-T, I-T): Using the T-configuration as the basis for responding to single-propeller power failure, the deformation modes are categorized into two types: H–T and I–T. When the rotorcraft is in the H or an approximate configuration and any of the power units fails, the H–T deformation mode can be executed. As shown in Fig. 5, the arm where the failed power unit is located rotates, bringing the failed power unit into the area enclosed by the three effective power units. During this process, the center of gravity of the rotorcraft should also remain within this area to ensure controllable attitude.

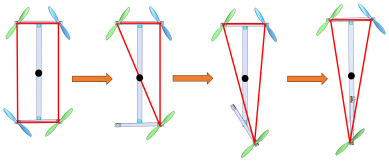

Fig. 5. Diagram of H-T transformation in configuration.

When the rotorcraft is in I or approximate configuration and the power unit fails, there are usually two scenarios: near-center power unit failure and far-center power unit failure, as shown in Fig. 6a and Fig. 6b. Near-center failure requires 90° arm rotation; far-center failure requires inward rotation, both maintaining CoG within the effective motor triangle.

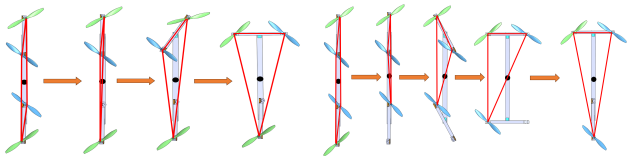

(a) Near-center failure (b) Far-center failure

Fig. 6. Diagram of I-T transformation in configuration.

III. Modeling, Control, and Power Distribution

Transformable rotorcraft have the ability to fly in different configurations, and changes in the position of the power motor and the angle of the tilt servo can cause changes in the tension arm and direction of the power rotor. Under the action of the configuration servo and tilt servo, the rotorcraft undergoes dynamic configuration changes, and the expected pose requires real-time response to various motion state variables such as body velocity and angular velocity, which can result in unstable or time-varying motion coupling relationships. In order to avoid complex modeling, control, and dynamic calculation, this paper analyzes the dynamic relationship of rotorcraft, adjusts typical configuration control parameters based on physical aircraft, calculates the motion characteristic values in transition control, calculates reliable control parameters, and then performs dynamic calculation based on proportional constraints for multi-modal configuration transformation.

A. Dynamic Relationship

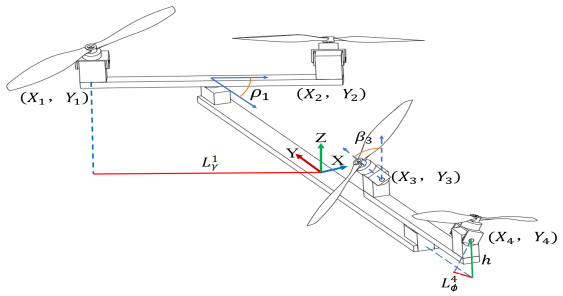

Fig. 7. Diagram of its axis-angle relationship.

Establish a body coordinate system with the midpoint of the fuselage as the origin $O_0 - X_0Y_0Z_0$, assuming that the center of gravity of the rotorcraft coincides with the origin of the coordinate system. The relationship between the body axes is shown in Fig. 7. Due to the limitation of the viewing angle, only one of some variables is schematically presented. The position of the power motor in the body coordinate system is as follows:

where ρ_1 and ρ_2 are the angles between the arms and the fuselage, and L is the length of the arm.

$$\begin{bmatrix} x_1 & y_1 \\ x_2 & y_2 \\ x_3 & y_3 \\ x_4 & y_4 \end{bmatrix} = \frac{L}{2} \begin{bmatrix} -\sin\rho_1 & \cos\rho_1 \\ \sin\rho_1 & -\cos\rho_1 \\ -\sin\rho_2 & -\cos\rho_2 \\ \sin\rho_2 & \cos\rho_2 \end{bmatrix} + \begin{bmatrix} 0 & L \\ 0 & L \\ 0 & L \\ 0 & L \end{bmatrix}, \quad (1)$$

The pitch, roll, and yaw moment arms are computed as follows:

$$L_\theta^i = L_\gamma^i = L \begin{bmatrix} \cos\rho_1 \\ \cos\rho_1 \\ \cos\rho_2 \\ \cos\rho_2 \end{bmatrix} + \frac{L}{2} \begin{bmatrix} 1 \\ -1 \\ 1 \\ -1 \end{bmatrix}, \quad (2)$$

$$L_\phi^i = h \begin{bmatrix} \sin\beta_1 \\ \sin\beta_2 \\ \sin\beta_3 \\ \sin\beta_4 \end{bmatrix} + \frac{L}{2} \begin{bmatrix} \sin\rho_1\cos\beta_1 \\ \sin\rho_1\cos\beta_2 \\ \sin\rho_2\cos\beta_3 \\ \sin\rho_2\cos\beta_4 \end{bmatrix}. \quad (3)$$

where β_j $(j = 1, 2, 3, 4)$ are the tilt servo rotation angles, and h is the vertical distance of the motor relative to the center of gravity.

Define motors No. 1 and No. 4 to turn counterclockwise, motors No. 2 and No. 3 to turn clockwise, and let F_j $(j = 1, 2, 3, 4)$ denote the pulling forces provided by

the four motors. The pitch, roll, and yaw torques are given by:

$$M_\theta = \sum_{j=1}^{4} \left(L_\theta^j F_j \cos\beta_j \right), \tag{4}$$

$$M_\phi = \sum_{j=1}^{4} \left(L_\phi^j F_j \cos\beta_j \right), \tag{5}$$

$$M_\gamma = \sum_{j=1}^{4} \left(M_j \sqrt{x_j^2 + y_j^2} \sin\beta_j + L_\gamma^j F_j \sin\beta_j \right). \tag{6}$$

The moments of inertia about the pitch, roll, and yaw axes are:

$$J_\theta = \sum_{i=1}^{4} m' X_i^2 + J'_\theta, \tag{7}$$

$$J_\phi = \sum_{i=1}^{4} m' Y_i^2 + J'_\phi, \tag{8}$$

$$J_\gamma = \sum_{i=1}^{4} m' \left(X_i^2 + Y_i^2 \right) + J'_\gamma. \tag{9}$$

where m' is the combined mass of the motor and tilt servo, and J'_θ, J'_ϕ, J'_γ represent the body's inherent moments of inertia.

The three-axis angular acceleration of pitch, roll, and yaw are as follows:

$$[\dot{\omega}_\theta,\ \dot{\omega}_\phi,\ \dot{\omega}_\gamma]^T = \left[\frac{M_\theta}{J_\theta},\ \frac{M_\phi}{J_\phi},\ \frac{M_\gamma}{J_\gamma} \right]^T \tag{10}$$

where:

- $\dot{\omega}_\theta$, $\dot{\omega}_\phi$, $\dot{\omega}_\gamma$ are the angular accelerations about the pitch, roll, and yaw axes, respectively,
- M_θ, M_ϕ, M_γ are the torques defined in (4)–(6),
- J_θ, J_ϕ, J_γ are the moments of inertia from (7)–(9).

B. Controller

The flight controller primarily controls the attitude of the rotorcraft and consists of an angle loop PID controller, an angular velocity loop PID controller, a power distribution controller, and a configuration-tilt angle controller, as shown in Fig. 8.

The desired angles (θ, ϕ, γ) for the pitch, roll, and yaw channels are inputted into the angle loop PID controller through remote control signals or the upper-level navigation control system. By combining the feedback of the current attitude angles of the rotorcraft in each axis, the desired attitude angular velocities are calculated $(\omega_\theta, \omega_\phi, \omega_\gamma)$, based on the desired angle ρ_i $(i = 1, 2)$ of the configuration servo and the tilt angle β_i $(i = 1, 2, 3, 4)$ of the power servo, as well as the feedback of the current attitude angular velocities of the rotorcraft in each axis, the angular velocity loop PID controller calculates the desired torques $(M_\theta, M_\phi, M_\gamma)$ for each axis of pitch, roll, and yaw based on the motion characteristics of the rotorcraft configuration. In the power distribution control section, by solving the matrix $\hat{f} = PQm$, the tension of each power propeller and the PWM drive signals for each power motor can be obtained.

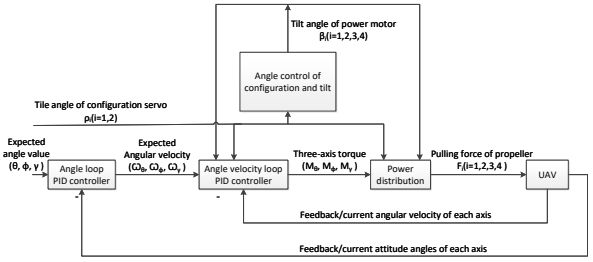

Fig. 8. Cascaded flight control architecture with configuration adaptation.

During dynamic reconfiguration, the time-varying moment of inertia and thrust arms necessitate an adaptive angular velocity controller. Based on the rotational dynamics relationship, motion characteristic values are defined for the three axes to capture the dependencies between thrust and angular acceleration.

The motion characteristic values for the three axes are defined as follows:

$$k_\theta = \frac{J_\theta}{\sum_{i=1}^{4} |L_\theta^i|}, \tag{11}$$

$$k_\phi = \frac{J_\phi}{\sum_{i=1}^{4} |L_\phi^i|}, \tag{12}$$

$$k_\gamma = \frac{J_\gamma}{\frac{M}{F} + \sum_{i=1}^{4} |L_\gamma^i|}. \tag{13}$$

Let k_θ^H, k_ϕ^H, k_γ^H, k_θ^I, k_ϕ^I, k_γ^I, and k_θ^T, k_ϕ^T, k_γ^T denote the motion characteristic values for the H-, I-, and T-configurations, respectively. The coefficients for transitional configurations are constructed as follows (using the H-I transformation as an example):

$$K_\theta = \frac{|k_\theta - k_\theta^I|}{|k_\theta - k_\theta^H| + |k_\theta - k_\theta^I|}, \tag{14}$$

$$K_\phi = \frac{|k_\phi - k_\phi^I|}{|k_\phi - k_\phi^H| + |k_\phi - k_\phi^I|}, \tag{15}$$

$$K_\gamma = \frac{|k_\gamma - k_\gamma^I|}{|k_\gamma - k_\gamma^H| + |k_\gamma - k_\gamma^I|}. \tag{16}$$

Let PID^H, PID^I, and PID^T represent the PID control parameters tuned in the H-, I-, and T-configurations, respectively. During the transition between H- and I-configurations, the PID control parameters are calculated as:

$$\mathrm{PID}_\theta = \mathrm{PID}_\theta^I K_\theta + \mathrm{PID}_\theta^H (1 - K_\theta), \tag{17}$$

$$\mathrm{PID}_\phi = \mathrm{PID}_\phi^I K_\phi + \mathrm{PID}_\phi^H (1 - K_\phi), \tag{18}$$

$$\mathrm{PID}_\gamma = \mathrm{PID}_\gamma^I K_\gamma + \mathrm{PID}_\gamma^H (1 - K_\gamma). \tag{19}$$

Similarly, the PID control parameters for transitions between H–T and I–T configurations can be calculated using the same method.

The determination of the tilt servo angles β_j is crucial for maintaining flight controllability during reconfiguration. Our analysis confirms that the design consideration of setting the maximum tilt angle to 25° aims to provide sufficient roll and yaw control authority. Analytical calculations show that at a 25° tilt angle, the motors sacrifice approximately 10% of the vertical lift, with about 42% of the total thrust allocated for generating roll moments. The configuration servo angle (ρ) is directly provided by the controller, and consequently, the tilt servo angle β_j is calculated according to Eq. (20).

$$\begin{aligned} &\beta = 30^\circ - \rho; \quad \rho \in [5^\circ; 30^\circ] \\ &\beta = 0^\circ; \quad \rho \in (30^\circ; 90^\circ] \end{aligned} \tag{20}$$

During the dynamic reconfiguration process of rotorcraft configurations, the moment of inertia and power arm of each axis undergo time-varying changes. Although PID algorithms can handle these variations, the tuning of fuzzy rule tables and the smooth control of rotorcraft deformation pose significant challenges in this study.

While advanced control methods such as FOPID [22] have demonstrated clear technical advantages in absolute performance and represent potential solutions for disturbance rejection in unmanned systems [23], addressing the real-time control requirements of rapidly reconfiguring, resource-constrained embedded systems necessitates a pragmatic approach. From the perspective of engineering applicability and system complexity trade-offs. Following previous work,the control parameter tuning method based on motion characteristic values is embedded into the controller design.

C. Power Distribution

The rotorcraft exhibits various asymmetric configurations during transitions between different modes, and the coupling relationship between motor thrust and flight attitude is complex and time-varying. To ensure the controllability of transition flight, reasonable power distribution is crucial. For the H-shaped transformable rotorcraft, this paper proposes a motor power distribution method suitable for asymmetric power layout, with the main contents as follows:

1) Selection of Coupling Parameters: Under the same magnitude of tensile force, the longer the force arm, the greater the torque generated, and the more significant the effect on the axial direction of the posture. The coupling parameters of the rolling force arm L_ϕ^i, pitching force arm L_θ^i, and yaw force arm L_γ^i acting on the rotorcraft by the motor tension are used to represent the degree of action of each motor tension on each attitude axis.

2) Construct Mapping Relationships: Construct a coupling parameter matrix P from L_ϕ^i, L_θ^i, L_γ^i, calculate the expected rotational torque of each axis M_θ, M_ϕ, M_γ by the controller, construct an input vector $\vec{m}$, and form an output vector $\vec{f}$ from the calculated tensile force F_i. Namely, P, $\vec{m}$ and $\vec{f}$ are respectively.

The power distribution relationship is expressed through the matrix equation:

$$P = \begin{bmatrix} L_\phi^1 & L_\theta^1 & L_\gamma^1 \\ L_\phi^2 & L_\theta^2 & L_\gamma^2 \\ L_\phi^3 & L_\theta^3 & L_\gamma^3 \\ L_\phi^4 & L_\theta^4 & L_\gamma^4 \end{bmatrix} \quad \vec{m} = \begin{bmatrix} M_\theta \\ M_\phi \\ M_\gamma \end{bmatrix} \quad \vec{f} = \begin{bmatrix} F_1 \\ F_2 \\ F_3 \\ F_4 \end{bmatrix} \tag{21}$$

3) Solving Decoupling Matrix: According to the input-output relationship of power distribution, there should exist $\vec{f} = PQ\vec{m}$, where Q is the corresponding decoupling matrix of the coupling parameter matrix P.

Generally, there is an infinite solution for the propeller pulling force towards the expected torque output. Here, we use the principle of competence that the longer the force arm, the greater the pulling force, to constrain and limit it, that is, the ratio of the pulling force of each propeller to the ratio of the force arms of each axis is proportional. Due to the different force arms of tension on different axes, it is impossible to simultaneously meet the limiting conditions, so power distribution design is carried out separately for each axis. Taking the rolling channel as an example.

There should be:

$$F_1 : F_2 : F_3 : F_4 = L_\phi^1 : L_\phi^2 : L_\phi^3 : L_\phi^4, \tag{22}$$

assuming:

$$F_i = K_\phi L_\phi^i \quad (i \in 1-4), \tag{23}$$

the rotational torque that can be obtained from the three axial directions is:

$$M_\phi^\phi = K_\phi \sum_{i=1}^{4} (L_\phi^i)^2, \tag{24}$$

$$M_\phi^\theta = K_\phi \sum_{i=1}^{4} L_\phi^i L_\theta^i, \tag{25}$$

$$M_\phi^\gamma = K_\phi \sum_{i=1}^{4} L_\phi^i L_\gamma^i. \tag{26}$$

Similarly, the torque requirements for pitch and yaw channels are allocated as $M_\theta^\phi, M_\theta^\theta, M_\theta^\gamma$ and $M_\gamma^\phi, M_\gamma^\theta, M_\gamma^\gamma$. Therefore, the total torque of the rolling channel is $M_\phi^\phi, M_\theta^\phi, M_\gamma^\phi$ and similarly, it can be obtained as follows:

$$\begin{bmatrix} M_\phi \\ M_\theta \\ M_\gamma \end{bmatrix} = \begin{bmatrix} M_\phi^\phi + M_\theta^\phi + M_\gamma^\phi \\ M_\phi^\theta + M_\theta^\theta + M_\gamma^\theta \\ M_\phi^\gamma + M_\theta^\gamma + M_\gamma^\gamma \end{bmatrix} = PP^T \begin{bmatrix} K_\phi \\ K_\theta \\ K_\gamma \end{bmatrix}, \tag{27}$$

where P is the coupling parameter matrix defined in Eq. (21).

Thus, there is a unique solution K that can be abbreviated as $K = (LL^T)^{-1}M$, further existence

$$F = L^T(LL^T)^{-1}M, \tag{28}$$

Among them, let $P = L^T$, then

$$Q = (P^TP)^{-1} \tag{29}$$

is the decoupling matrix.

4) Propeller Thrust Calculation: Thus, the thrust F_i of each motor at any desired torque $\vec{m}$ under any configuration P can be directly calculated. The thrust F_i is accumulated with the throttle value thr and assigned to the motor.

It is worth noting that the obtained tension values F_i may not be entirely usable and may exceed the actual range that can be provided. There are two main reasons for this:

- The rolling channel is prone to a maximum force arm that is too small, and when attempting to achieve a certain amount of torque output in this axis, it may exceed the actual tension range.
- The yaw channel is prone to having all the positive and negative signs of the force arms being the same, making $F_i + thr$ less than zero, this means that the motor is reversing, but generally the direction of the aircraft motor cannot be changed.

Therefore, rules should be established during the configuration transformation to limit the angles of the configuration servo and the tilting servo within a certain range, in order to adjust the coupling matrix and avoid the above two situations. The roll, pitch, and yaw force arms should be balanced and symmetrical, meeting the following conditions:

$$\begin{aligned} |L_\phi^1 + L_\phi^3| &= |L_\phi^2 + L_\phi^4| \\ |L_\theta^1 + L_\theta^2| &= |L_\theta^3 + L_\theta^4| \\ |L_\gamma^1 + L_\gamma^3| &= |L_\gamma^2 + L_\gamma^4| \end{aligned} \tag{30}$$

IV. Experimental Verification and Analysis

1) Investigating the high passability motion conditions of rotorcraft through continuous motion experiments in confined spaces.
2) Experimental investigation of fault-tolerance flight via single-propeller power failure response.
3) Assessing the torque characteristic of rotorcraft through torque testing.

A. Narrow-gap Crossing Experiment

Under normal circumstances, rotorcraft fly in an H-shaped power layout. When encountering narrow gaps during flight and needing to cross, they can enter the H-I deformation mode. The maximum horizontal size of the rotorcraft can be reduced to 44.2% of the general flight configuration (H-shape), providing high passability motion conditions. As shown in Fig. 9, the rotorcraft had taken off from the H-configuration, undergoes dynamic reconstruction in the air in a parallelogram configuration to transform into the I-configuration, and then maintains the configuration attitude to complete continuous narrow gap crossing flight. As shown in Fig. 10, The rotorcraft took off at 2.5 s, reconfigured to I-shape by 3 s, began forward motion at 5.5 s, aligned laterally at 8.4 s, traversed the gap by 9 s, and landed at 10 s. The flight height had been controlled at around 0.6 m throughout the entire process. The horizontal dimension of the narrow gap had been set to 37 cm, The lateral displacement data deviation during gap traversal can be controlled within 4 cm, and the rotorcraft had achieved good position control conditions based on previous attitude control experiments.

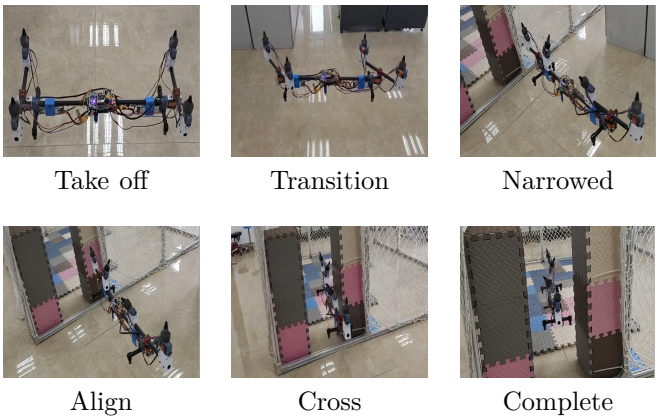

Fig. 9. Continuous motions in confined space

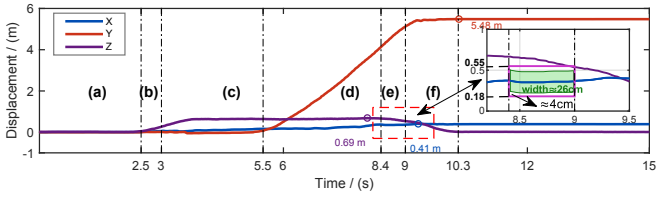

Fig. 10. Position data of continuous motion in confined space.

B. Fault-tolerant Flight Experiment

Our fault-tolerant strategy reconfigures the rotorcraft to a T-shaped configuration, relocating the failed motor centrally. The remaining three motors provide lift, with the tail motor's tilt servo generating yaw torque to maintain control. Specifically, after a power unit fails, the rotorcraft can change its configuration to a T-shaped configuration, placing the failed power unit in the center, with the remaining three power units forming a tritor. The yaw axis torque is generated by the tail tilt servo. It is worth noting that the overall lift source of the rotorcraft changes from four motors to three motors, so each motor lift needs to be correspondingly increased, and the increase in lift for the tail motor should be greater.

1) T-configuration Under Single Propeller Power Failure: To validate fault-tolerant flight under the T-shaped power layout, an on-board start-stop experiment with a 20-second cycle was conducted in the near-center power section under the T-configuration, to test and investigate the power supply and distribution of the rotorcraft during the transition from four motors to three motors.

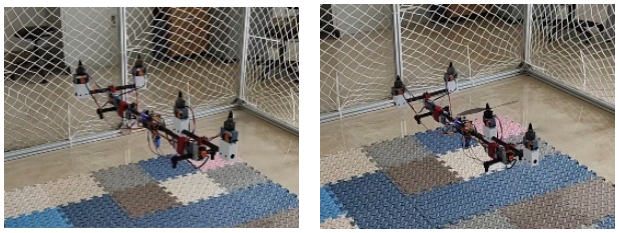

(a) Supply of four power units (b) Power unit shut-down near the center

Fig. 11. The single power in-flight shutdown under T-configuration.

The experiment primarily focuses on the data before and after the shutdown of the power unit, as illustrated in Fig. 12. The rotorcraft had taken off at 0 s and reached the predetermined altitude at 2.83 s, with the pitch angle controlled within the interval of [1°,-0.5°]. Subsequently, at 12.67 s, the near-center power unit had been shut down, causing the pitch angle to suddenly oscillate within the interval of [-2.1°,-1.8°], for a duration of 2.33 s. This oscillation is primarily due to the transition from four-motor to three-motor power distribution. Afterwards, the pitch angle of the rotorcraft had returned to stability, and the data exhibits periodicity. The results of the intermittent shutdown experiments indicate that the transition switching between the two power distribution modes is overall smooth.

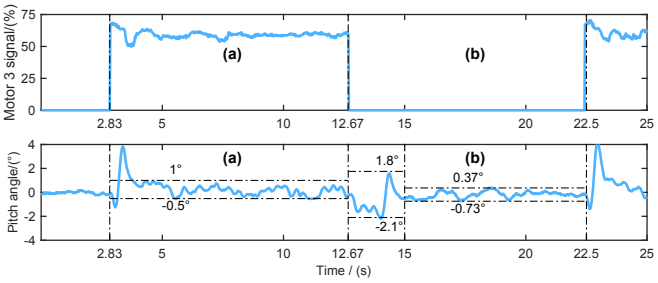

Fig. 12. Attitude data during single-propeller shutdown.

2) Transition Control for Single-Propeller Power Failure in Arbitrary Configurations: Taking the general H-shaped configuration as an example, when the angle between the arm and the fuselage is at its maximum 90°, if one of the power units is suddenly shut down during stable flight in this configuration, the corresponding arm will immediately rotate to place the power unit near the center of the fuselage. Fig. 13 illustrates the experimental situation of fault-tolerant flight through configuration transition in the event of a single-propeller power failure.

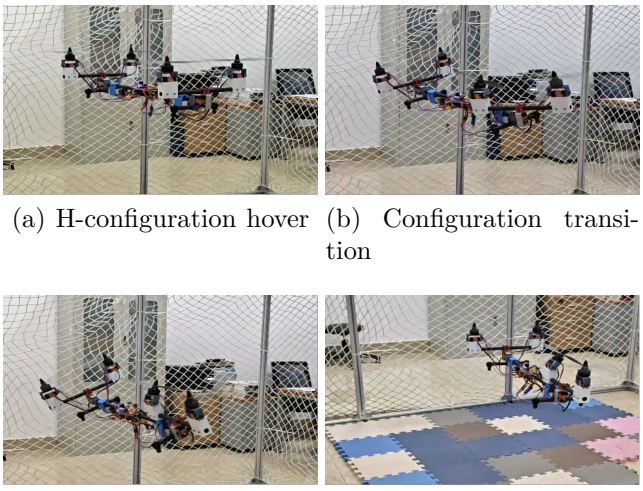

(a) H-configuration hover (b) Configuration transition

(c) Attitude adjustment (d) Stability control

Fig. 13. Fault tolerant control through configuration transformation.

Fig. 14 corresponds to the axial data of the rotorcraft's attitude in the experiment shown in Fig. 13. The rotorcraft had started hovering in an H-shaped configuration at 0 s, and a single-propeller power failure had occurred at 1.8 s. The rotorcraft immediately had transitioned to a T-shaped configuration and performed attitude adjustment. The entire fault-tolerant flight process through configuration transformation lasts for 1.2 s, during which the roll channel had experienced a significant angle tilt in the [24°, -21°] range, and the maximum angle tilt in the pitch channel was 10.7°. Then, it had been transformed to the T-configuration and returned to stability. The experiment had proved the feasibility of using T-configuration transformation to deal with single propeller dynamic failure.

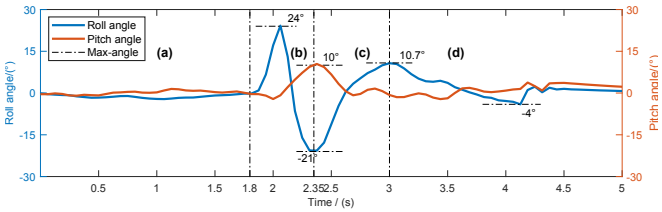

Fig. 14. Attitude curve under the motor failure.

C. Torque Characteristic Test

When dealing with valve switching torsion scenarios, the rotorcraft can be transformed into I configuration and further increase the angle of the tilt servo to enhance the external torque in the yaw direction. As shown in Fig. 15a, the rotorcraft had been fixed above the torque tester, and the tilt servos of the front and rear arms had been tilted in different directions.

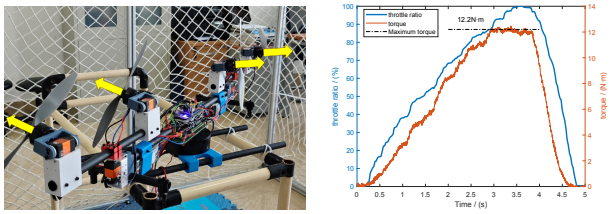

(a) Torque test (b) Torque of yaw channel

Fig. 15. Torque characteristic.

As shown in Fig. 15b, The externally applied torque in the yaw direction had increased with the increase of throttle value. When the motor had reached its maximum speed in the figure, the overall torque provided by the rotorcraft has been 12 $\mathrm{N}\cdot\mathrm{m}$, the rotorcraft can provide the torque output required to rotate the specific valve.

V. Conclusion

We have designed and constructed an H-shaped multi-modal transformable rotorcraft. Through adjustments in the structural and power layout, the rotorcraft maintains favorable conditions for high-passability morphing while addressing the issue of time-varying center of gravity during flight. Based on motion characteristic values, we tuned the PID control parameters, and to accommodate limited computational resources, we proposed a competency-based power distribution strategy with proportional constraints on force and moment arms, thereby achieving stable dynamic reconfiguration in flight. Furthermore, we developed a flight fault-tolerant scheme that employs a T-shaped transformation for dynamic fault response, thus ensuring stable rotorcraft control in the event of a single-rotor power failure.

Future Work:Subsequent research will focus on developing robust control-oriented dynamic distribution methods for multi-modal transformation and further exploring dynamic reconfiguration strategies to enhance the adaptability and reliability of the rotorcraft in complex environments.

References

[1] X. Zhang, C. Xie, S. Liu, M. Yan, and S. Xing, "Development requirements and challenges of intelligent morphing aircraft," Acta Aeronaut. Astronaut. Sin., vol. 44, no. 21, pp. 8–34, 2023, (in Chinese).

[2] J. Dai, X. Kang, Y. Song, and J. Wei, Reconfigurable Mechanisms and Reconfigurable Robots: Kinematic Analysis, Synthesis and Control Based on Bifurcation Evolution. Beijing, China: Higher Education Press, 2021, (in Chinese).

[3] A. Briod, P. Kornatowski, J.-C. Zufferey, and D. Floreano, "A collision resilient flying robot," J. Field Robot., vol. 31, no. 4, pp. 496–509, 2014.

[4] S.-J. Kim, D.-Y. Lee, G.-P. Jung, and K.-J. Cho, "An origami-inspired, self-locking robotic arm that can be folded flat," Sci. Robot., vol. 3, no. 16, p. eaar2915, 2018.

[5] E. Sihite, A. Kalantari, R. Nemovi, A. Ramezani, and M. Gharib, "Multi-modal mobility morphobot (m4) with appendage repurposing for locomotion plasticity enhancement," Nat. Commun., vol. 14, no. 1, p. 3324, 2023.

[6] K. Kim, P. Spieler, E.-S. Lupu, A. Ramezani, and S.-J. Chung, "A bipedal walking robot that can fly, slackline, and skateboard," Sci. Robot., vol. 6, no. 59, p. eabf8136, 2021.

[7] K. Hang, X. Lyu, H. Song, J. A. Stork, A. M. Dollar, D. Kragic, and F. Zhang, "Perching and resting—a paradigm for uav maneuvering with modularized landing gears," Sci. Robot., vol. 4, no. 28, p. eaau6637, 2019.

[8] N. Bucki and M. W. Mueller, "Design and control of a passively morphing quadcopter," in Proc. IEEE Int. Conf. Robot. Autom. (ICRA), 2019, pp. 4643–4649.

[9] A. Sakaguchi and K. Yamamoto, "A novel quadrotor with a 3-axis deformable frame using tilting motions of parallel link modules without thrust loss," IEEE Robot. Autom. Lett., vol. 7, no. 4, pp. 9581–9588, 2022.

[10] J. Sugihara, T. Nishio, K. Nagato, M. Nakao, and M. Zhao, "Design, control, and motion strategy of TRADY: Tilted-rotor-equipped arial robot with autonomous in-flight assembly and disassembly ability," 2023.

[11] M. Zhao, K. Kawasaki, X. Chen, S. Noda, K. Okada, and M. Inaba, "Whole-body aerial manipulation by transformable multirotor with two-dimensional multilinks," in Proc. IEEE Int. Conf. Robot. Autom. (ICRA), 2017, pp. 2245–2249.

[12] F. Ruiz, B. Arrue, and A. Ollero, "SOPHIE: Soft and flexible aerial vehicle for physical interaction with the environment," 2022.

[13] N. Bucki, J. Tang, and M. W. Mueller, "Design and control of a midair-reconfigurable quadcopter using unactuated hinges," IEEE Trans. Robot., vol. 39, no. 1, pp. 539–557, 2023.

[14] D. Falanga, K. Kleber, S. Mintchev, D. Floreano, and D. Scaramuzza, "The foldable drone: A morphing quadrotor that can squeeze and fly," IEEE Robot. Autom. Lett., vol. 3, no. 2, pp. 209–216, 2018.

[15] Y. Bai and S. Gururajan, "Evaluation of a baseline controller for autonomous "figure-8" flights of a morphing geometry quadcopter: Flight performance," Drones, vol. 3, no. 3, p. 70, 2019.

[16] M. Zhao, K. Kawasaki, K. Okada, and M. Inaba, "Transformable multirotor with two-dimensional multilinks: modeling, control, and motion planning for aerial transformation," Adv. Robot., vol. 30, no. 13, pp. 825–845, 2016.

[17] M. Zhao, T. Anzai, F. Shi, X. Chen, K. Okada, and M. Inaba, "Design, modeling, and control of an aerial robot DRAGON: A dual-rotor-embedded multilink robot with the ability of multi-degree-of-freedom aerial transformation," IEEE Robot. Autom. Lett., vol. 3, no. 2, pp. 1176–1183, 2018.

[18] M. Zhao, T. Anzai, K. Okada, and M. Inaba, "Singularity-free aerial deformation by two-dimensional multilinked aerial robot with 1-dof vectorable propeller," 2021, preprint.

[19] M. Zhao, K. Okada, and M. Inaba, "Enhanced modeling and control for multilinked aerial robot with two dof force vectoring apparatus," IEEE Robot. Autom. Lett., vol. 6, no. 1, pp. 135–142, 2021.

[20] ——, "Versatile articulated aerial robot DRAGON: Aerial manipulation and grasping by vectorable thrust control," Int. J. Robot. Res., vol. 42, no. 4-5, pp. 214–248, 2023.

[21] G. E. M. Abro, V. S. Asirvadam, S. A. B. Zulkifli, and S. A. Raza, "Review of hybrid control designs for underactuated quadrotor with unmodelled dynamic factors," in Emerging Technol. Comput., ser. Lecture Notes Inst. Comput. Sci., Social Inform. Telecommun. Eng., vol. 357, 2020, pp. 62–85.

[22] G. E. M. Abro, A. M. Abdallah, and M. E. Elshaar, "Helical trajectory control of quadrotor uavs using fractional order proportional-integral-derivative FOPID controller," in Proc. IEEE Int. Conf. Autom. Sci. Eng. (CASE), 2024, pp. 2085–2090.

[23] G. E. M. Abro, V. S. Asirvadam, S. A. B. M. Zulkifli, A. Sattar, D. Kumar, and A. Anwer, "Effects of unmodelled dynamic factors on an under-actuated quadrotor: A review of hybrid observer design methods," Meas. Control, vol. 53, no. 9-10, pp. 1978–1987, 2020.